Available online at www.sciencedirect.com
SCIENCE DIRECT®

Journal of the European Ceramic Society 24 (2004) 495–506

www.elsevier.com/locate/jeurceramsoc

Microstructure and phase morphology of wood derived biomorphous SiSiC-ceramics

Cordt Zollfrank*, Heino Sieber

Department of Materials Science, Glass and Ceramics, University of Erlangen-Nuernberg, D-91058 Erlangen, Germany

Abstract

Biomorphous SiSiC-ceramics were prepared by spontaneous Si-melt infiltration of beech and pine wood derived biocarbon templates (C_B-templates) at 1550 °C for 1 h. The microstructure, phase distribution and interface morphology of the anisotropically structured, microcellular SiSiC-ceramic composite were investigated by X-ray diffraction (XRD) as well as by light, scanning and, in detail, by transmission electron microscopy (LM/SEM/TEM). The biomorphous SiSiC-ceramics consist of three different phases: solidified Si in the cell lumina, few residual carbon islands located in the middle of the former wood cell walls and two different, reaction-formed SiC-morphologies. While the majority of the SiC-phase exhibits a grain diameter of a few microns, a second nano-grained SiC-phase was identified at the interface between the coarse-grained SiC-phase and the residual biocarbon. The occurrence of the nano-grained SiC-phase is related to the density and pore size of the initial C_B-template. While in large pores and narrow carbon struts (low density earlywood) of the C_B-template an excess of Si-melt yields the formation of mainly the coarse-grained SiC-phase, in latewood sections (small pores and thick C-struts) of the biocarbon template the nano-grained SiC-phase forms layers of up to several μm in thickness. Due to the uni-directional pore structure of the wood derived C_B-templates, the morphology of the biomorphous SiSiC-ceramics can be analysed in well-defined pore orientations. A microstructural model for the SiC-formation and phase growth will be proposed and discussed with respect to conventional processed SiSiC-materials.

Keywords: Biomorphous ceramics; Biotemplating; SiC; Transmission electron microscopy

1. Introduction

SiC-based ceramics and composite materials exhibit attractive properties like excellent mechanical strength at high-temperature, high thermal conductivity and good oxidation as well as corrosion resistance. Therefore, SiC- and SiSiC-materials are currently intensively studied for a broad variety of uses ranging from dense materials for frictional and structural application,[1–3] to materials with a defined porosity for high-temperature filter or catalyst support structures.[4,5]

The reactive infiltration of carbonaceous materials with liquid Si (LSI-process) represents an interesting processing scheme for SiSiC-materials regarding economical and technological aspects[6] and results in a nearly dense ceramic matrix composite (CMC). Well known materials are REFEL SiC[7] and SILCOMP SiC/Si[8] as well as carbon fibre reinforced SiC-CMCs.[9] The LSI-process is also suitable for preparing near net-shape ceramic composites for structural applications. Manufacturing of reaction infiltrated, net-shape SiSiC-based composites[10,11] as well as the fabrication of functionally graded SiSiC-composites using novel three-dimensional printing techniques[12] have been described. However, the microstructural design of the SiSiC-composite materials is limited and depends mainly on the applied technique for preparation of the SiC/C-preform, which is subsequently subjected to the LSI-process. While extrusion techniques for manufacturing of SiSiC-monoliths are restricted to cell diameters down to below 1 mm, an uniaxial directed pore geometry on the micrometer level cannot be prepared by conventional techniques.

The use of biostructures such as wood for the preparation of microcellular designed ceramic materials has become a matter of increasing interest in the recent years. Various attempts have been made to utilise native as well as pre-processed biological plant materials (lignocellulosics) for preparation of carbon monoliths[13] as well as for biomorphous oxide or SiC-based ceramic materials.[14–16] The morphology of natural plants is characterised by different cellular and microporous structures ranging from the nanometre to the millimetre scale.[17] The major

* Corresponding author.

0955-2219/03/$ - see front matter © 2003 Elsevier Ltd. All rights reserved.
doi:10.1016/S0955-2219(03)00200-0

biopolymeric constituents of wood are cellulose, hemicellulose, and lignin. Cellulose chains are bundled to fibrils and form a bioorganic, cellulose-fibre reinforced composite material in a matrix of lignin and hemicellulose. The average elemental composition of wood is approximately 50 wt.% C, 43.4 wt.% O, 6.1 wt.% H, 0.2 wt.% N and 0.3 wt.% of inorganic materials.[17]

Biomorphous, microcellular SiSiC-ceramics can be manufactured by liquid Si-infiltration of the carbonised tissue of lignocellulosics.[18] The LSI-processing of plant derived biocarbon templates (C_B-templates) is able to reproduce the micro-morphology of the native tissue with high precision in the SiSiC-ceramic composite, thus representing a net-shape process on the micrometre scale.[14] This process yields SiSiC-ceramic materials with a unidirectional microstructure and anisotropic structural and mechanical properties. Since the work of Byrne and Nagle,[19] biomorphous SiSiC-ceramics derived from wood have been studied intensively over the last years.[20–25] The fabrication involves the preparation of porous biocarbon monoliths by pyrolysis of the native plant materials, which are subsequently subjected to the liquid Si-infiltration. The processing yields biomorphous, dense or less porous SiSiC-ceramics, depending on the kind of the used wood species. In contrast to the Si-melt infiltration, highly porous, single phase, biomorphous SiC-ceramics can be manufactured by reactive infiltration of gaseous Si-containing reactants like Si/SiO-vapour or silanes.[26–28] Due to their anisotropic morphology with an unidirected pore structure on the micrometre level, biomorphous SiC- and SiSiC-ceramic composites are interesting candidates for applications as e.g. liquid metal filters, high-temperature catalyst support or nozzle structures and micro-reactor devices.

However, the microscopical mechanism and kinetic constraints, which govern the infiltration and reaction processes as well as the SiC-phase growth and microstructure development during liquid Si-infiltration of biomorphous or conventional carbon preforms are not fully understand yet. Contrary to the technical importance of the liquid Si-infiltration processing, only few investigations are available dealing with the microstructural investigation of the phase development on the micro- and sub-micrometer scale. The aim of the present study is a detailed investigation of the micro morphology, the phase composition and interface structure of biomorphous SiSiC-ceramic composites manufactured by the LSI-process from biological derived C_B-templates of beech and pine wood.

2. Experimental procedure

Biocarbon templates (C_B-templates) were prepared from oriented solid wood samples (axial, radial, tangential: $50\times20\times20$ mm^3, Fig. 1). The wood specimens were dried (105 °C, 15 h) and pyrolysed in N_2-atmosphere in an electrical heated furnace. A slow heating rate of 1 K/min was applied up to 500 °C to prevent macro-cracking. At this temperature the wood polysaccharides (cellulose, hemicellulose) and the lignin were decomposed to carbon. A following heating rate of 5 K/min up to the peak temperature of 800 °C was then applied. The peak temperature of 800 °C was maintained

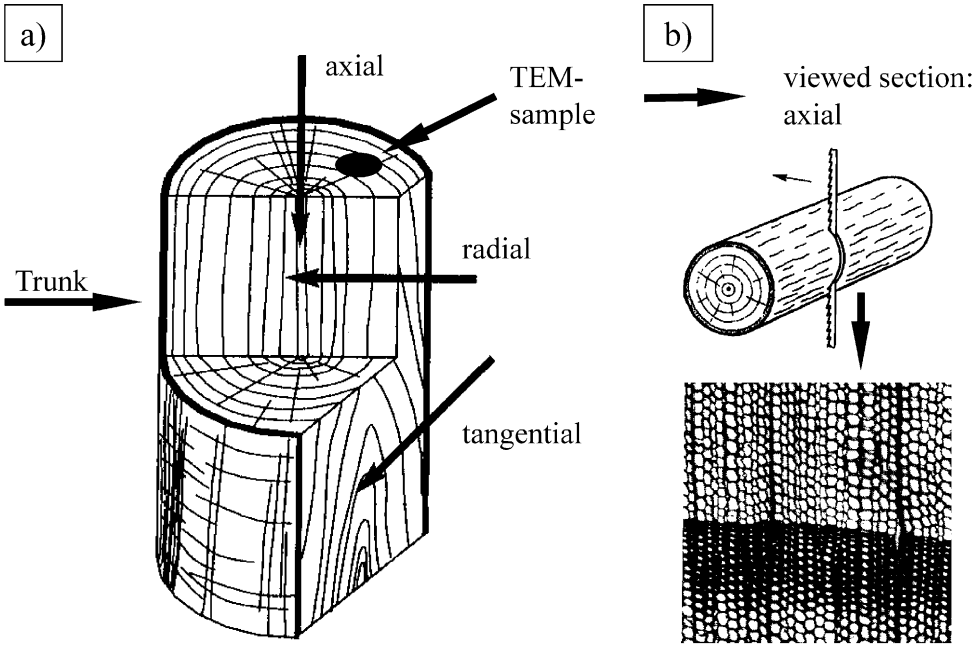

Fig. 1. Schematic sketch of (a) the definition of the major sections cut from wood in respect to the growth directions and (b) the axial section used in this study for LM, SEM and TEM observations.

for 4 h. After pyrolysis, the cell walls of the native wood were converted into carbon struts with a thickness of a few micrometres. Details of the processing scheme, the materials properties of the C_B-template, the shrinkage and the weight loss during pyrolysis were described in Refs. 20 and 22. Subsequently, the carbonised C_B-templates were infiltrated in an electrically heated furnace in a carbon crucible at 1550 °C in vacuum with liquid Si (Si-powder 99%, d_{50} = 6.8–7.6 μm, Silgrain, Wacker, Germany) for 1 h according to procedures previously published.[20]

The microstructures of the intermediate and final products were characterised by scanning electron microscopy (SEM, Stereoscan S 250 MK3, Cambridge Instruments, Cambridge, UK) in the BSE- (back-scattered electron) and the SE- (secondary electron) mode as well as by elemental analysis by EDX/SEM. The crystalline phases were determined by X-ray diffraction using CuK_α radiation (XRD, D 500, Siemens, Karlsruhe, Germany). Light micrographs of the ion-milled samples were obtained with a Zeiss Axiophot equipped with a digital camera.

For transmission electron microscopy (TEM) investigations, sections of the SiSiC-ceramic specimens were cut from the axial planes of the sample with a thickness of 1 mm using a diamond coated circular saw, Fig. 1. Discs with a diameter of 3 mm were obtained using an ultrasonic disc cutter (Gatan, model 601). The discs were polished on one side with various diamond laps and cloths. Afterwards, the sample was turned and mechanically ground to a thickness of approximately 60 μm. Further thinning and polishing was performed using a dimple grinder (Gatan, model 656) until the Si- and the SiC-phases became transparent at a thickness of approximately 6 μm. Ion-beam thinning on a precise ion polishing system (PIPS, Gatan, model 691, Ar-ions) at 5 kV at an angle of 5° ensured electron transparency. The samples were investigated in a Zeiss EM10A transmission electron microscope operated at 80 kV and in a Phillips CM30 operated at 300 kV for bright field imaging. EDX-spectra in the TEM (CM30) were performed at 200 kV using a SiLi-detector (type 7370, ISIS 30, Link, Oxford, UK).

3. Results

Biocarbon template structures (C_B-templates) were manufactured from oriented solid wood samples of beech (*Fagus sylvatica*) and pine (*Pinus sylvestris*) by pyrolysis in N_2-atmosphere (Fig. 2a and c). Beech wood

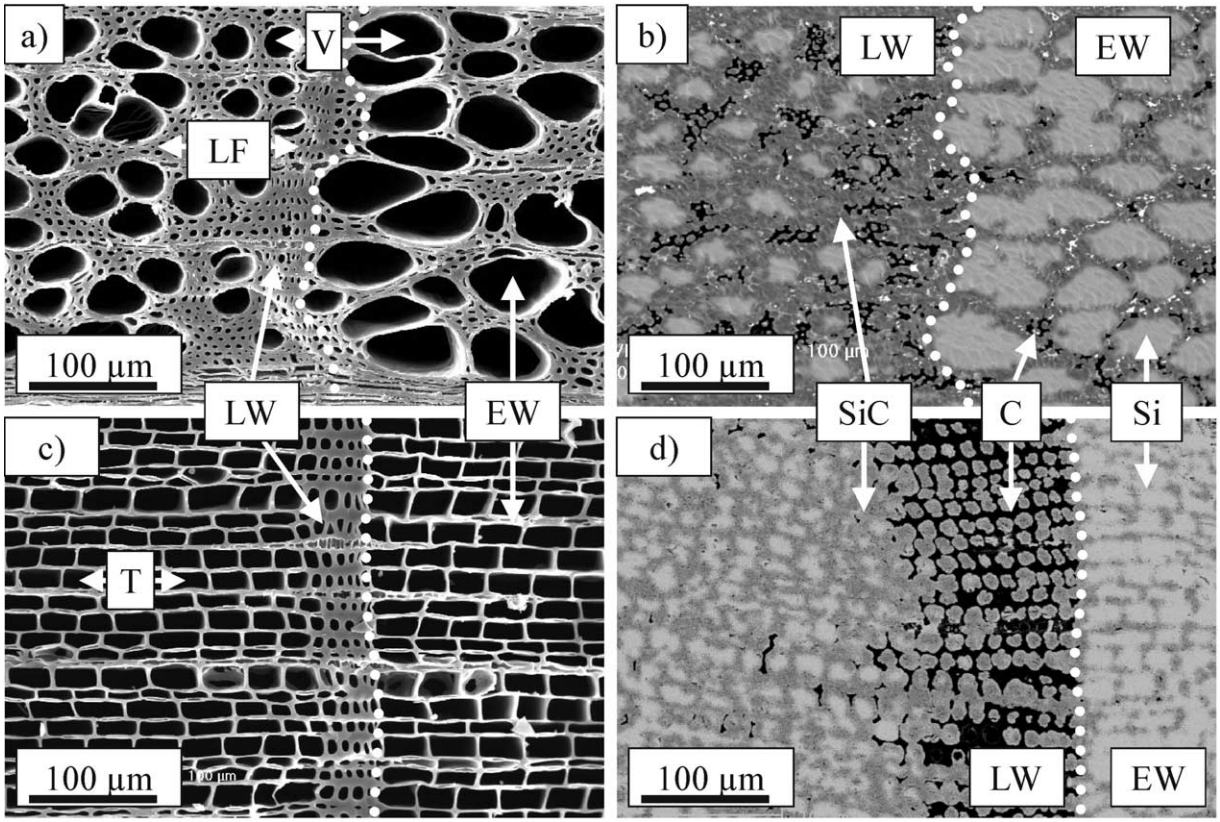

Fig. 2. SEM-micrographs (a) of the C_B-template of beech wood after pyrolysis at 800 °C (SE), (b) biomorphous SiSiC-ceramic derived from beech after LSI at 1550 °C (BSE), (c) of the C_B-template of pine wood after pyrolysis at 800 °C (SE), (d) biomorphous SiSiC-ceramic derived from pine after LSI at 1550 °C (BSE). EW: earlywood, LW: latewood, LF: libriform fibres, V: vessels, T: tracheids, C: carbon, Si: silicon, SiC: silicon carbide, dotted line: border of annual ring.

is less homogeneous than pine wood and consists of (i) basic tissue with libriform fibres (LF) and (ii) vessel (V) elements, which form long tubes of up to 100 μm in size and a length of a few centimetres (Fig. 2a). Pine wood shows a more uniform structure and consists of 90–95% tracheids (T), which are long and slender cells tapered at the ends with a diameter up to 50 μm and a length up to few mm[29] (Fig. 2c). The tracheids and tracheary elements in pine and beech wood are oriented in the direction of the trunk axis. Regions of varying porosity are found within an annual ring in the native wood and also in the pyrolysed samples (Fig. 2a and c) which are formed throughout the growth period within 1 year. In beech wood, large vessels are observed in the earlywood (EW) with an average diameter of approximately 50–80 μm, whereas the size of the vessel lumina in latewood (LW) is much smaller (approximately 20–50 μm). The cell wall thickness in the basic tissue of beech wood varies from 3 to 8 μm. Only small differences are observed in EW and LW in respect to the dimensions of the basic tissue. In pine wood, the EW is formed in spring with a cell wall thickness of approximately 3 μm and lumina of approximately 40 μm, whereas the LW appears with much thicker cell walls (approximately 6–10 μm) and smaller lumina (approximately 3–20 μm).

Native beech as well as pine wood exhibits a total mass loss of approximately 70–74 wt.% after pyrolysis.[20] With a given C-content of 50% in the native wood only the half of this carbon remain in the C_B-template. After pyrolysis the densities of the C_B-templates are 0.55 g/cm^3 for beech and 0.31 g/cm^3 for pine wood char. Also an anisotropic shrinkage in the principal growth directions of the wood is observed. The axial shrinkage accounts for 22%, whereas in the radial and tangential directions higher values are observed (30 and 36% respectively). Beech and pine wood shrinkage is of the same magnitude (Table 1).

According to the conventional processing of SiSiC-materials,[7] spontaneous infiltration of the C_B-templates starts as soon as the used Si-powder is molten [M_P(Si) = 1414 °C]. The infiltration rate depends on the size of the pores, the viscosity of the Si-melt, the height of Si-melt within the compact and the Si-wettability of the C_B-template.[20] Molten Si at the processing temperature of 1550 °C exhibits a sufficient low viscosity and good wettability to cause rapid infiltration into the C_B-template. After Si-infiltration the carbon struts of the former wood cell walls are reacted into β-SiC.

Table 1
Properties of the C_B-templates after pyrolysis at 1800 °C in N_2-atmosphere, adapted from ref. 20

Wood	Beech	Pine
Pyrolysis weight loss (wt.%)	74.2	73.8
Pyrolysis shrinkage (%)		
Axial	22	23
Radial	32	28
Tangential	38	31
Density (g/cm^3)		
Pyrolysed	0.55	0.31

The SEM-micrographs in Fig. 2b and d show an overview of the beech and pine wood derived SiSiC-ceramics after the LSI-process. The light grey areas in Fig. 2 are assigned to Si, which is solidified in the previously empty lumina of the wood cells. The dark grey phase corresponds to the formed SiC and the black regions are unreacted carbon. In the SEM-micrograph of the beech wood sample, a few bright white spots were visible (Fig. 2b). EDX-analysis of these inclusions revealed, that the major constituent was Fe. The total amount of this phase in the samples accounted for about 1–2 wt.%, and is due to impurities in the used Si-powder.

The borders of the annual wood growth rings of the initial wood structures are clearly visible in the biomorphous SiSiC-ceramics (dotted line in Fig. 2). The EW and LW regions are discernible in the SEM-micrographs. The fraction of residual carbon is high in LW areas, whereas in the EW areas unreacted carbon is found only in the dense basic tissue in case of the beech wood. The small pores of the LW areas in both wood species are clogged by formed SiC, free Si is not observed in these regions. The narrow carbon struts of the EW in pine wood are completely transformed into SiC.

After the LSI-process, all pores up to a pore diameter of approximately 50 μm are filled up with residual Si (e.g. beech wood vessels). However, also some cell lumina with a diameter of about 100 μm are filled with Si. The biomorphous SiSiC-ceramic derived from pine wood shows a phase composition of approximately 60 vol.% SiC, 30 vol.% free Si, and 10 vol.% of residual carbon, whereas the composition of the SiSiC-beech was approximately 57 vol.% SiC, 38 vol.% free Si, and 5 vol.% residual carbon. Both specimens exhibit a porosity of about 5–10%. The porosity, Si-content and the residual carbon of the final microcellular SiSiC-composites depend significantly on the specific anatomy of the wood preform. In beech wood, the dense basic tissue is more equally distributed over the annual ring. The dense carbon regions are smaller in diameter compared with the LW regions of pine. Thus, less residual carbon is found in the SiSiC-ceramics derived from beech wood compared to the pine wood specimen. Highly dense carbon regions in pine wood are only found in the LW areas, where most of the residual carbon is located. Contrary, a large amount of free Si is found in the large vessels of the beech wood template and less free Si is observed in SiSiC-ceramics derived from pine wood due to the smaller pores.

The macroscopic appearance of the biomorphous SiSiC-ceramic composites after ion-milling (for preparation of TEM-specimens) is shown in the LM-micrographs (Fig. 3). It is obvious, that the cellular morphology of native wood appears to be fully retained in the ceramic composite. In the TEM-specimens, the Si-phase is sputtered away from the cell lumina to a higher extent as the SiC-phase from the cell struts during ion-milling, because the sputter coefficient of Si is considerably higher than for SiC. Thus, formation of holes is observed in the Si-filled lumina, whereas the SiC-struts remain relatively dense. After the Si has been removed from the cell lumina, highly porous, fragile and brittle SiC-struts are left over, which require special care in further handling for TEM-observation.

Fig. 4a shows the TEM-overview of the biomorphous SiSiC-ceramic derived from beech wood and in Fig. 4c derived from pine wood. Three different phases could be distinguished by selected area diffraction (SAD) and energy-dispersive X-ray (EDX) measurements. The dark phase in the TEM-micrographs corresponds to dense SiC. Faceted SiC-grains are located at the areas of the former wood cell walls. The previously empty cell lumina of the C_B-template are filled with solidified Si after the infiltration process. Contour lines due to variable thickness are visible in the Si, however, most of the Si-phase has already sputtered away due to the ion milling during TEM sample preparation. An additional nano-crystalline SiC-phase was detected between the coarse SiC-grains and the residual carbon at higher magnification (Fig. 4b and d).

SAD studies on arbitrary selected coarse SiC-grains located at the edge of the cell lumina in the basic tissue of the biomorphous SiSiC-ceramic derived from beech wood exhibited a preferential orientation of the SiC in the [110] and [112] crystallographic zones (Fig. 5). It should be noted, that in some cases the solidified Si adopts the same crystal orientation as the SiC. However, we are aware that the TEM- and SAD-analysis provides only local crystallographic information.

The third phase specified appears with uniform bright contrast between the SiC-grains, and it is located in the middle of the former carbon struts. This phase is assigned to residual carbon, which had not been reacted. The residual carbon in the samples appears to be amorphous. By means of SAD only a diffuse halo was observed (see inset in Fig. 6). High magnification studies showed the amorphous character of the biocarbon phase (Fig. 6). The amount of residual carbon in the specimens depends on the location in the biomorphous

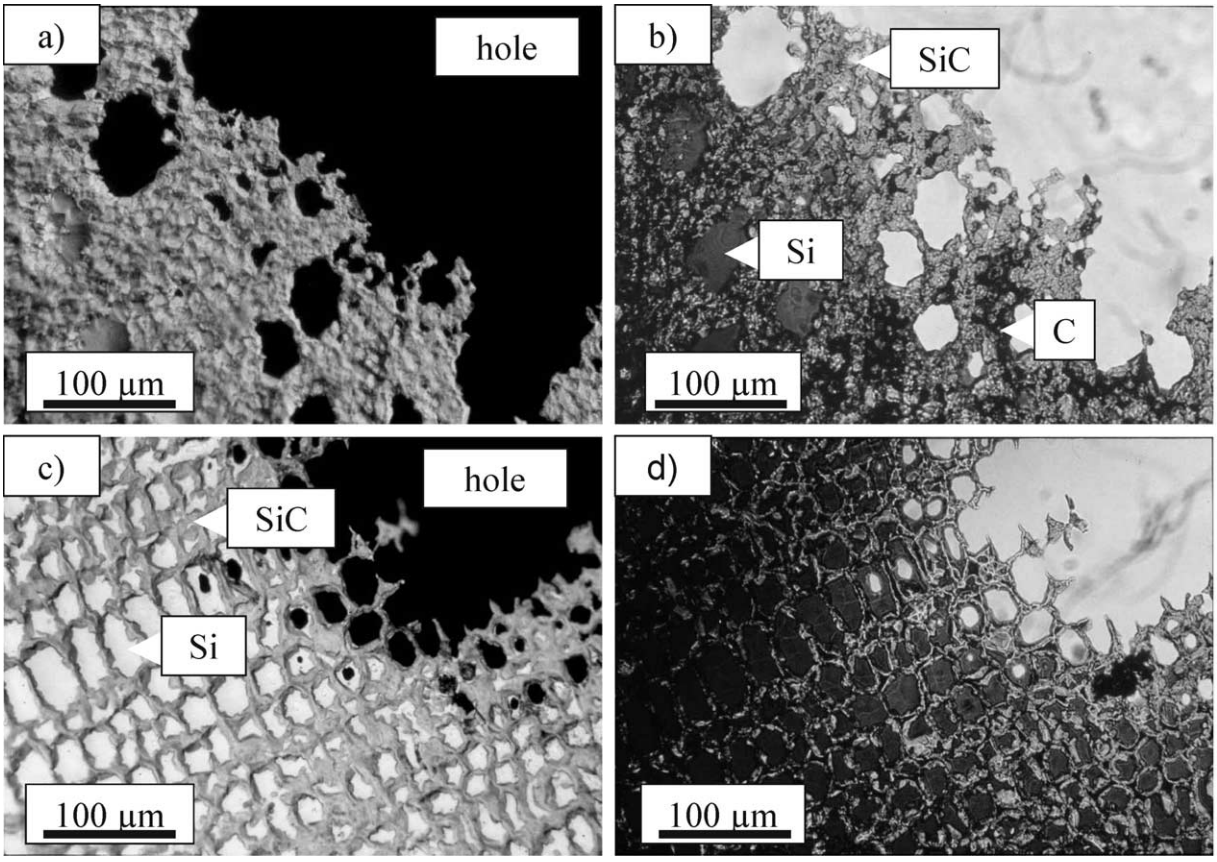

Fig. 3. LM-micrographs after ion-milling: (a) axial-view of biomorphous SiSiC-ceramic derived from beech wood and (b) in transmission mode, (c) axial-view of SiSiC-ceramic derived from pine and (d) in transmission mode. The sample were prepared for TEM-observation. In the transmission LM-micrographs free Si appears from dark to bright red. The SiC becomes transparent and the C remains opaque.

SiSiC-ceramic specimen. In regions with a higher carbon density of the initial C_B-template (e.g. LW in the pine char derived SiSiC-ceramics) the fraction of unreacted carbon is higher compared to the EW regions, where most of the carbon has been reacted into large SiC-grains (Fig. 7). Only very few residual carbon as well as nano-crystalline SiC-phase could be detected in the EW regions in the TEM-micrographs. In LW regions of the biomorphous SiSiC-ceramics with a higher residual carbon density the fraction of the nano-crystalline SiC-phase is also higher. However, the nano-crystalline SiC-phase is only found at the carbon/coarse-grained SiC interface. It forms a dense, nearly continuous layer between the surface of the former carbon struts and the coarse-grained SiC-phase. In some areas the nano-crystalline SiC-phase nearly completely surrounds the residual carbon islands (Fig. 7b).

Fig. 8 shows an overview of the nano-crystalline SiC-phase at higher magnification. The ring diffraction pattern displays an isotropic distribution of the nano-SiC, without preferred orientation (see inset in Fig. 8). The bright spots present in the SAD-diagram may be derived from nearby coarse-grained SiC. The thickness of the nano-grained SiC-layer between the carbon and the coarse SiC-grains varies from 0.1 up to several μm. The average crystallite grain size found ranges from 40 to 100 nm. The occurrence of a nano-grained SiC-phase has been described before for Si-melt infiltrated carbon fibre performs.[37] Nano-sized β-SiC with a grain diameter in the order of 100 nm was found at the surface of the carbon fibres and appeared to be distributed in the solidified Si. Contrary to this, in the case of biomorphous SiSiC-ceramics, the nano-grained SiC-phase forms a dense layer between the residual carbon and the SiC-

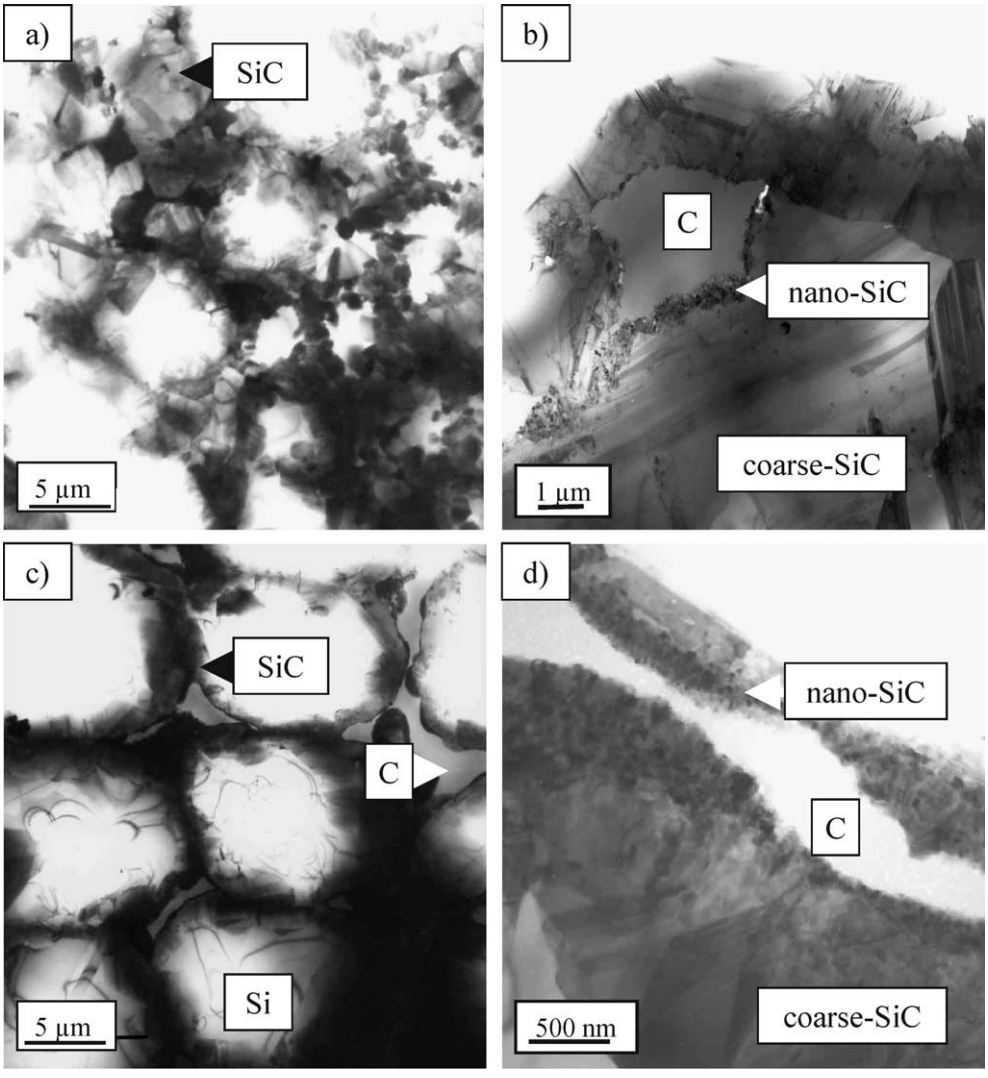

Fig. 4. TEM-micrographs of biomorphous SiSiC-ceramics showing the microstructure of oriented, axial sections: (a) SiSiC derived from beech wood, (b) same sample as in (a) observed at higher magnification, (c) SiSiC derived from pine wood and (d) same sample as in (c) observed at higher magnification; the grey phase with contour lines is Si filling the cell lumina, the dark grey phase represents reacted SiC-struts, the light grey phase corresponds to residual carbon.

matrix. Fig. 8 also shows, that the nano-sized SiC-grains exhibit well defined facets. A high number of stacking faults is observed within the crystals. Stacking faults in β-SiC are known to be related to the SiC-formation kinetics.[31] In the biomorphous SiSiC-ceramics, an orientational relationship between individual nano-sized SiC-particles could not be detected. Note that stacking faults were also observed in the coarse-grained SiC-phase. It should be also denoted, that the grain sizes of the nano SiC-phase and the coarse SiC-grains exhibit a bimodal distribution. SiC-grains with intermediate sizes could not be observed. Thus, the formation of the coarser SiC-grains by a simple growth of the nano-grained SiC-phase may not occur.

Fig. 9a shows the interfaces of the nano-grained SiC-phase to the residual carbon phase at high magnification. An additional interphase at the nano-SiC/C interface could not be observed. The results match the observation described by Schulte-Fischedick,[32] who also observed a sharp nano-SiC/carbon interface in carbon fibre reinforced SiC-CMCs. The nano-SiC/coarse-SiC interface is depicted in Fig. 9b. The transition from the nano- to the coarse-grained SiC is extremely sharp. SiC-phase grain with intermediate sizes or additional interphases could not be observed.

An analytical EDX-line-scan over the two interfaces of the nano-grained SiC-phase is shown in Fig. 10. The line-scan was performed from the coarse-grained SiC-phase over the nano-grained SiC-phase into a residual carbon island. In an overall EDX-spectrum of that area only X-ray peaks derived from Si and C were observed. The intensities of the C- and the Si-signals remain unchanged by scanning over the two different SiC-phases. Thus, the element composition of the two areas should be similar. At the nano-SiC/C interface the Si-signal decreases to zero with a slight slope over a width of 100 nm, whereas the C derived signal is increased in the same region. The slope of the signal is observed, because the electron beam and the interface are not aligned parallel to each other. As already stated above, additional interphases between the coarse-SiC/nano-SiC and the C_B/nano-SiC interfaces are not detected. The increased C-intensity at the ends of the line-scans is due to the accumulation of electron beam activated carbon.

4. Discussion

The infiltration of C_B-templates with liquid Si yields a SiSiC-ceramic material with a SiC-matrix pseudomorphous to the initial wood cell anatomy with embedded Si. Coarse β-SiC-grains with diameters up to 15 μm replaced the carbon struts of the C_B-template. Due to the high porosity of the C_B-template, the biomorphous SiSiC-ceramics contains a higher excess of residual Si (between 30 and 38 vol.% for the investigated pine and beech derived SiSiC) compared to conventionally processed SiSiC-material (e.g. REFEL SiC: approximately

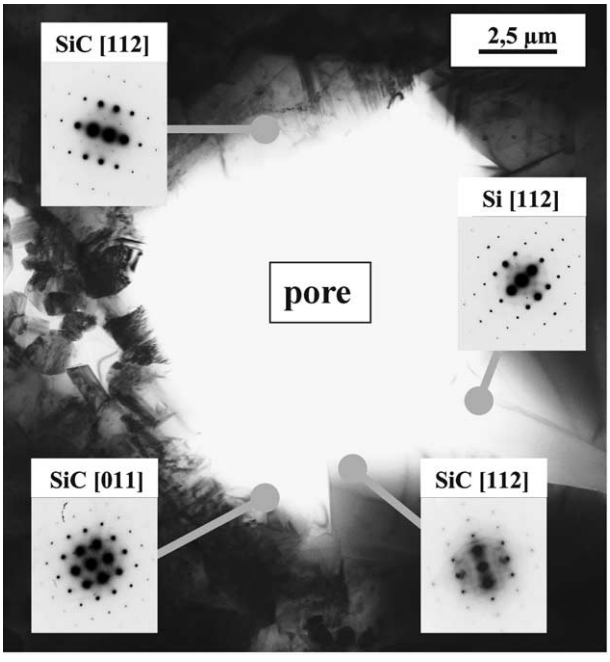

Fig. 5. TEM-micrograph and selected area diffraction (SAD) analysis of the coarse-grained SiC-phase in biomorphous SiSiC-ceramics. Shown are the lumen of a LF filled with Si and the reacted SiC struts consisting of coarse SiC-grains at the former cell wall.

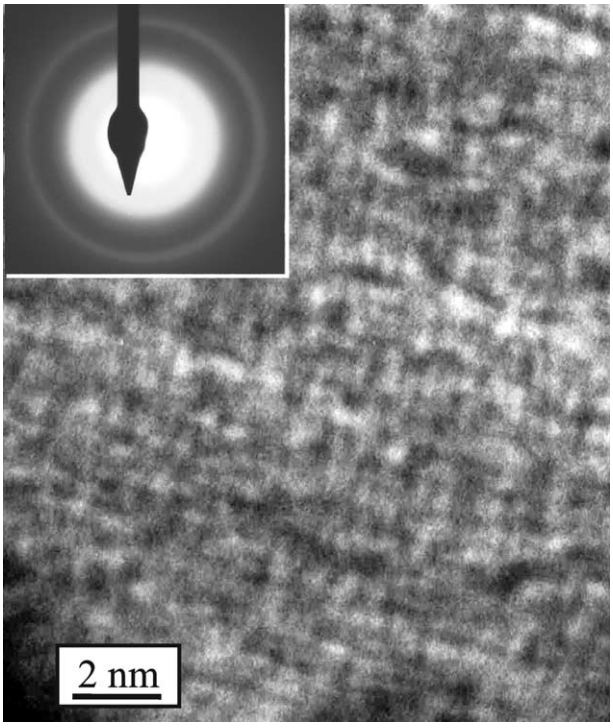

Fig. 6. High magnification TEM-micrograph and SAD analysis of the residual biocarbon in biomorphous SiSiC-ceramics. The SAD ring pattern proves the amorphous character of the material (inset).

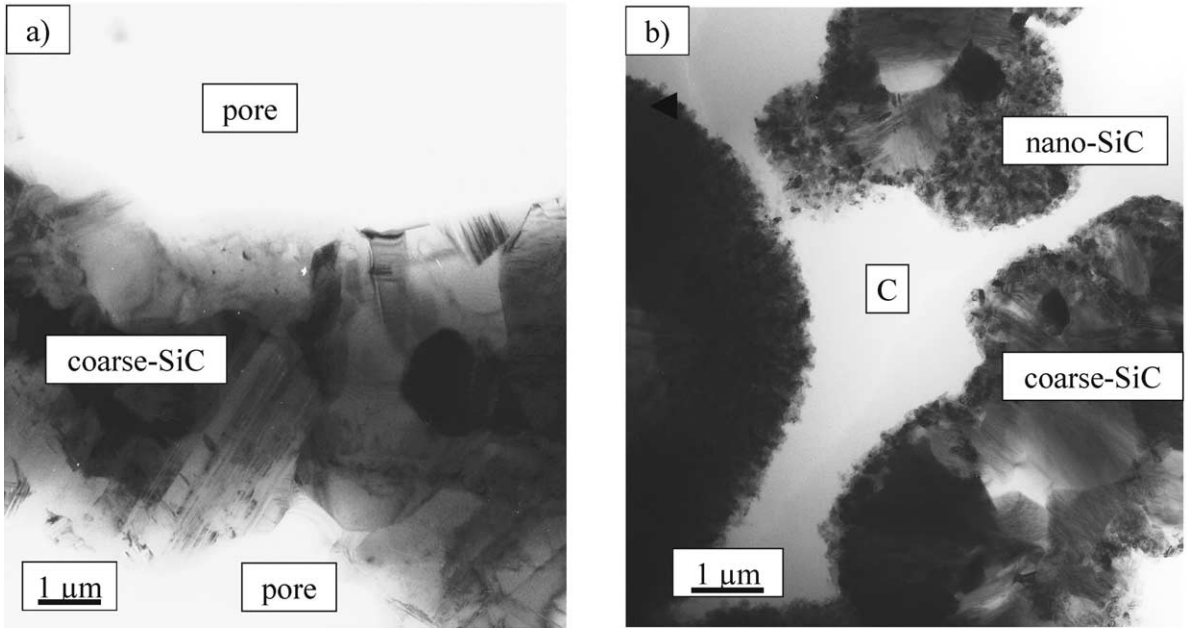

Fig. 7. TEM-micrograph of beech wood derived SiSiC: (a) coarse-grained SiC-phase replacing a carbon strut in the EW region; residual carbon is not present, (b) nano-grained SiC-phase forming a layer of about 1 µm and surrounding a coarse SiC-grain in the LW area.

10 vol.%).[30] After the Si-infiltration only small amounts of residual carbon remained in the biomorphous SiSiC-specimens. The residual carbon appears to be fully amorphous, the SAD pattern showed diffuse halos. Even at high magnifications in the TEM-micrographs no graphitic structures could be observed. The graphitisation of wood char requires temperatures higher than 1800 °C.[33,34] It is more likely, that the carbon of the wood char is of turbostratic amorphous character in an early stage of maturation.[35]

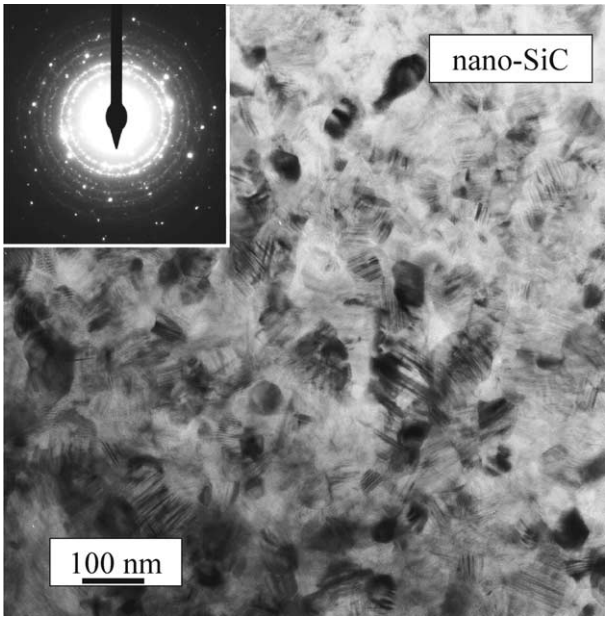

Fig. 8. TEM-micrograph and SAD-diagram (inset) of the nano-grained SiC-phase in biomorphous SiSiC-ceramics, an inner part of the former cell wall is shown. The strong reflections visible in the SAD-diagram are derived from vicinal coarse SiC-grains.

The Si-infiltration and reaction kinetics by spontaneous wetting of biocarbon template structures was analysed by Greil et al.[20] The Si-infiltration rate and depth strongly depends on the pore diameter. For a given pore diameter of 1–10 µm, the carbon template is spontaneously infiltrated with liquid Si within 10–1 s, if the depth of infiltration is assumed to be 0.1 m. The SiC-formation kinetics is limited by diffusion of the reaction partners through the formed SiC-reaction layer after Si-melt infiltration and an initial phase of the reaction. The estimated diffusion times at 1600 °C given in literature vary from 4.8 h for a protective SiC-diffusion barrier thickness of 1.5 µm in Si-melt infiltrated SiC-coated carbon fibres,[36] to 40 min for the complete transformation of a carbon strut with thickness of 10 µm into SiC in biomorphous SiSiC-ceramics.[20] We found that the carbon of the EW region with a strut thickness of 3 µm and rectangular pores (pine char, Fig. 1a) was fully transformed into SiC within 1 h of processing time at 1550 °C. On the other hand, the LW regions in the pine wood char with a carbon strut thickness of 6–10 µm (see pine char, Fig. 1a) and small pores (3–20 µm) exhibit large areas of unreacted carbon.

Similar findings were observed for the beech wood template. In both seasonal regions of the beech wood char, basic tissue with very small pores (1–7 µm) and thick carbon struts (2–7 µm) are observed. The carbon struts in this basic tissue areas were not quantitatively

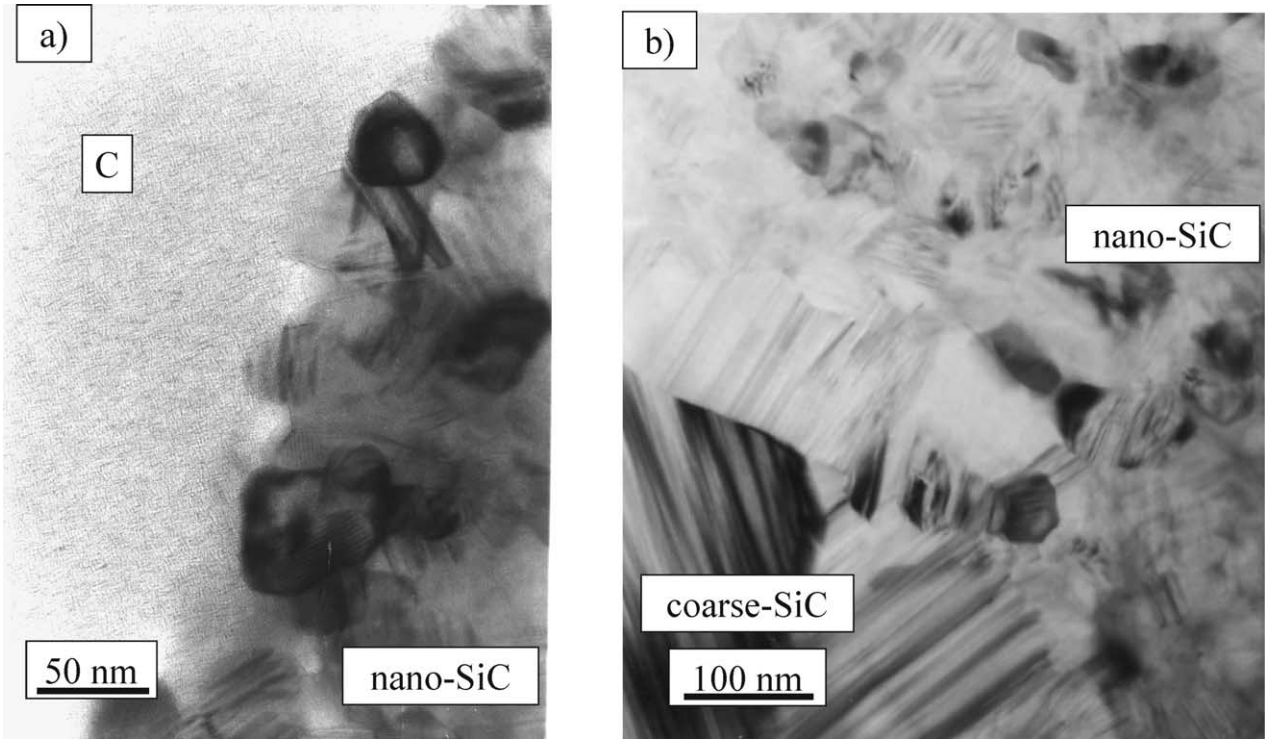

Fig. 9. High-magnification TEM-micrographs of the nano-grained SiC-phase interfaces in biomorphous SiSiC-ceramics derived from beech wood: (a) interface of the nano-SiC/C_B-phase, (b) interface of the coarse-grained SiC/nano-grained SiC-phase.

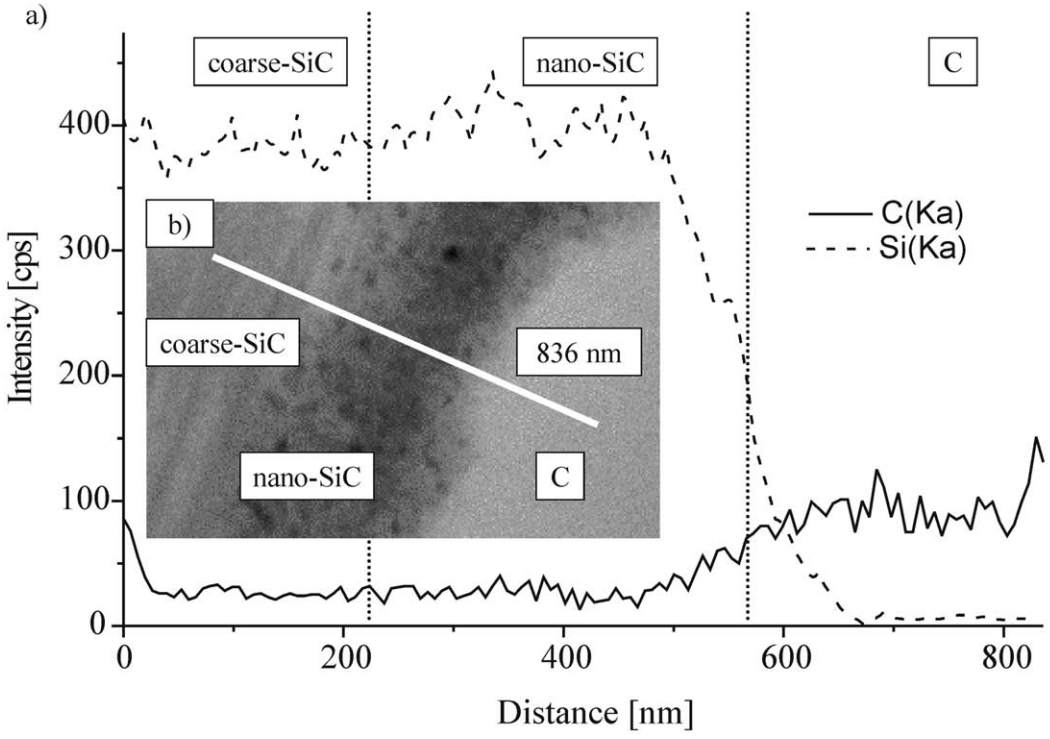

Fig. 10. (a) EDX-line-scan over the interface of the coarse-SiC/nano-SiC interface and the nano-SiC/C_B interface; (b) STEM-image of the area, where the line scan was measured. The length of the scan was 836 nm. The observed sample is derived from beech wood.

converted into SiC in EW as well as in LW regions. In both wood char samples, the residual carbon appears to be encapsulated by nano-sized SiC-grains. It can be concluded, that regions with high porosity and narrow struts are more easily reacted than more dense areas with thick struts under identical process conditions. This behaviour is due to the fact, that the coarse-grained SiC-phase grows from the carbon strut into the liquid Si-filled pores during the reaction, similar to the reaction of carbon fibres with the Si-melt described by Pampuch et al.[37] The SiC-growth results in a clogging of the small pores once a certain amount of carbon is consumed from the struts. The access of fresh, additional liquid Si is subsequently inhibited and the reaction stops. This is particularly observed in the small pores of the LW regions of both wood species and also counts for the dense basic tissue of the beech wood template. On the other hand, the large pores of the EW regions can not be blocked by SiC-grains, because the supply of carbon is limited due to the narrow carbon struts, which will be consumed in short reaction times. These regions exhibit an almost quantitative reaction of the biocarbon into coarse-grained SiC.

TEM-analysis of the microstructure showed a large content of an additional SiC-morphology formed during the Si-melt infiltration process. A nano-grained SiC-layer with an average particle diameter of 40–100 nm was observed at the C_B/SiC interfaces. Nano-grained SiC-phase regions were never found at the Si/SiC interfaces. Similar results regarding different SiC-morphologies were described by Sawyer and Page[38] as well as by Ness and Page[30] for the Si-infiltration of graphite preforms. In a recent paper, Schulte-Fischedick et al.[32] described a nano-grained SiC-layer at the C/SiC interface by TEM-observation of liquid Si-infiltrated C/C_f preforms. However, the nano-crystalline SiC-phase observed by Pampuch et al.[37] appears to be disseminated within the Si-matrix. This observation does not match the morphology found in the biomorphous SiSiC-ceramics. The nano-grained SiC-phase is clearly divided from the Si by coarse-grained SiC. In the biomorphous SiSiC-ceramics we have found only coarse SiC-grains at the Si/SiC interface. The observed coarse-grained SiC/nano-grained SiC interface seems to corresponds to the former carbon boundary of the C_B-template at intermediate stages of the SiC-formation. The phase arrangements and micro-morphology in the biomorphous SiSiC-ceramics is similar to the SiC-morphologies described for the liquid Si-infiltrated C/C_f preforms.[32]

The large β-SiC-grains exhibit a single crystalline spot diffraction pattern, although a high amount of stacking faults is observed within the grains. The observed high fraction of stacking faults within the coarse-SiC cannot be explained satisfactory at this stage. The highly exothermic, fast reaction together with a high proportion of nucleation sites present in the C_B-template may be the reason for the observed fraction of stacking faults. When nano-grained SiC is formed in the initial stage of the reaction, many stacking faults are inserted, because of the lack of time necessary to adopt the lowest-energy structure.[39] The same is true for the dissolution/re-crystallisation process during formation of the coarse SiC-grains. From the fact, that coarse SiC-grains are always found between the nano-grained SiC-layer and the Si-melt, it can be concluded, that these grains are not newly nucleated from the reaction with the biocarbon, but were grown on or from the nano-grained SiC-phase by the dissolution/re-crystallisation processes. Since the SiC-precipitation process is also fast,[37] stacking faults in the coarse-SiC are likely to be introduced.

At the nano-SiC/C_B- and the nano-SiC/coarse-SiC interfaces no additional interphases could be detected neither at high magnification nor by means of EDX-spectroscopy. The C_B/nano-SiC interface is sharp edged. This gives rise to the consideration, that the nucleation of nano-grained SiC may have occurred at the very beginning of the Si-infiltration and also at a later stage within the carbon by diffusion of Si through the SiC-layer barrier formed in the initial stages of the reaction. The observed transition of the grain size between the coarse-grained SiC-phase and nano-grained SiC-phase is abrupt. Thus, a dissolution of the nano-grained SiC-phase and a re-crystallisation process on the coarse SiC-grains has to be assumed. However, for a complete understanding of the microstructure evolution in the SiSiC-ceramics, more detailed investigations of the SiC-phase formation kinetics at different time steps during the liquid Si-infiltration reaction are necessary.

5. Conclusions

Microcellular SiSiC-ceramics can be prepared from porous C_B-templates by spontaneous Si-melt infiltration at 1550 °C. The overall microscopic morphology of the biomorphous SiSiC-ceramics is similar to materials manufactured by the conventional LSI-process and consists of three different phases: SiC from the reaction of Si with the biomorphous carbon, solidified Si filling the pores of the initial wood structure and isolated regions of amorphous, residual carbon. The SiC-phase exhibits two different morphologies: coarse β-SiC-grains with average grain diameters of about 15 μm at the Si/SiC interface and a nano-grained SiC-phase with average diameters below 100 nm, located only at the C_B/SiC-interface. Residual carbon exist in high-density regions of the former wood structure, they are often completely covered by the nano-grained SiC-phase, forming isolated islands of up to 5 μm in size. The evolution of the different phases during the LSI-processing of the wood derived C_B-templates is a combined infiltration/

reaction process influenced by the local carbon morphology as well as on time-dependent dissolution, recrystallisation and SiC-grain growth processes.

The amount of the individual phases (Si, SiC, C) as well as the micro-morphology in the biomorphous SiSiC-ceramics strongly depends on the structure of the biological char template, especially the local porosity and carbon strut thickness due to the seasonal growth pattern of the wood. While thin carbon struts (<3 μm) in high porosity regions results in a completely reacted SiSiC-material with coarse SiC-grains, large Si and small residual carbon amount, low porosity preform materials with thick carbon struts (>3 μm) yields a high fraction of unreacted carbon together with nano-grained SiC-phase and a smaller proportion of embedded Si. Here, the coarse-grained SiC-phase clogs the small pores and inhibits further Si-infiltration and reaction. By selecting appropriate C_B-templates designed SiSiC- or SiSiC/C-materials in respect to their microstructure can be developed.

Acknowledgements

The financial support of the Volkswagen-Foundation under contract #I/73 043 and the German Science Foundation (DFG) under contract SI 773/1-1 is appreciated. The TEM work was carried out in the Central Facility for High Resolution Electron Microscopy (Philips CM30, EDX) and the Institute for Pharmaceutical Biology (Zeiss EM 10) of the Friedrich-Alexander University Erlangen-Nuernberg, Germany. The authors are also grateful to Christiane Hoffmann for performing the infiltration experiments and to Petra Rosner, Gerhard Frank and Peter Greil for discussions.

References

1. Krenkel, W. and Henke, T., Design of high performance CMC brake discs. *Key Eng. Mat*., 1999, **164**, 421.
2. Wilhelm, M., Kornfeld, M. and Wruss, W., Development of SiC-Si composites with fine-grained SiC microstructures. *J. Eur. Cer. Soc*., 1999, **19**, 2155.
3. Paris, J. Y., Vincent, L. and Denape, J., High-speed tribological behaviour of a carbon/silicon-carbide composite. *Comp. Sci. Tech*., 2000, **61**, 417.
4. Kawamura, H., Application of structural ceramics in ceramics engines and diesel particulate filter (DPF). *Ind. Cer*., 1999, **19**, 200.
5. Droschel, M., Hoffmann, M. J., Oberacker, R., von Both, H., Schaller, W., Yang, Y. Y. and Munz, D., SiC-ceramics with tailored porosity gradients for combustion chambers. *Key Eng. Mat*., 2000, **175**, 149.
6. Gern, F. H. and Kochendorfer, R., Liquid silicon infiltration: Description of infiltration dynamics and silicon carbide formation. *Composites A*, 1997, **28**, 355.
7. Hillig, W. B., Melt infiltration approach to ceramic matrix composites. *J. Am. Ceram. Soc*., 1988, **71**, C96.
8. Popper, P., The preparation of dense self-bonded silicon carbide bodies. In *Special Ceramics*. Heywood, London, 1960, p. 209.
9. Fitzer, E., Gadow, R. and Speicher, M., Fiber-reinforced silicon carbide. *Am. Cer. Soc. Bull*., 1986, **65**, 326.
10. Greil, P., Near net shape manufacturing of ceramics. *Mat. Chem. Phys*., 1999, **61**, 64.
11. Hozer, L., Lee, J. R. and Chiang, Y. M., Reaction infiltrated, net-shape SiC composites. *Mat. Sci. Eng. A*, 1995, **195**, 131.
12. Moon, J., Caballero, A. C., Hozer, L., Chiang, Y. M. and Cima, M. J., Fabrication of functionally graded reaction infiltrated SiC-Si composite by three-dimensional printing (3DP^{TM}) process. *Mat. Sci. Eng. A*, 2001, **298**, 110.
13. Byrne, C. E. and Nagle, D. E., Carbonized wood monoliths—characterisation. *Carbon*, 1997, **35**, 26.
14. Greil, P., Biomorphous ceramics from lignocellulosics. *J. Eur. Ceram. Soc*., 2001, **21**, 105.
15. Sieber, H., Rambo, C., Cao, J., Vogli, E. and Greil, P., Manufacturing of porous oxide ceramics by replication of wood morphologies. *Key Eng. Mat*., 2002, **206–213**, 2009.
16. Ota, T., Takahashi, M., Hibi, T., Ozawa, T., Suzuki, S., Hikichi, Y. and Suzuki, H., Biomimetic Process for Producing SiC "Wood". *J. Am. Ceram. Soc*., 1995, **78**, 3409.
17. Gibson, L. J., Wood: a natural fibre reinforced composite. *Metals and Materials*, 1992, **8**, 333.
18. Byrne, C.E. and Nagle, D.E., *Carbonized Wood and Materials Formed Therefrom*. Pat. US6051096, 1996; Pat. US6124028, 1998.
19. Byrne, C. E. and Nagle, D. E., Cellulose derived composites—a new method for materials processing. *Mat. Res. Innovat*., 1997, **1**, 137.
20. Greil, P., Lifka, T. and Kaindl, A., Biomorphic silicon carbide ceramics from wood: I. and II. *J. Eur. Ceram. Soc*., 1998, **18**, 1961.
21. Shin, D. W. and Park, S. S., Silicon/silicon carbide composites fabricated by infiltration of a silicon melt into charcoal. *J. Am. Ceram. Soc*., 1999, **82**, 3251.
22. Sieber, H., Hoffmann, C., Kaindl, A. and Greil, P., Biomorphic cellular ceramics. *Adv. Eng. Mater*., 2000, **2**, 105.
23. Martinez-Fernandez, J., Valera-Feria, F. M. and Singh, M., High-temperature compressive mechanical behaviour of biomorphic silicon carbide ceramics. *Scripta Mater*., 2000, **43**, 813.
24. Singh, M., Environment conscious ceramics (Ecoceramics). In *Ceramic Engineering and Science Proceedings, 21, 24th Annual Conference on Composites, Advanced Ceramics, Materials, and Structures: B*, ed. T. Jennsen and E. Usundag. The American Ceramic Society, 2000, p. 39.
25. Guanjun, Q., Rong, M., Ning, C., Chunguang, Z. and Zhihao, J., Microstructure transmissibility in preparing SiC ceramics from natural wood. *J. Mat. Proc. Tech*., 2002, **120**, 107.
26. Vogli, E., Mukerji, J., Hoffman, C., Kladny, R., Sieber, H. and Greil, P., Conversion of oak to cellular silicon carbide ceramic by gas-phase reaction with silicon monoxide. *J. Am. Ceram. Soc*., 2001, **84**, 1236.
27. Vogli, E., Sieber, H. and Greil, P., Biomorphic SiC-ceramic prepared by Si-vapor phase infiltration of wood. *J. Eur. Ceram. Soc*., 2002, **22**, 2663.
28. Sieber, H., Vogli, E., Mueller, F., Greil, P., Popovska, N., Gerhard, H. and Emig, G., Gas phase processing of porous, biomorphic SiC ceramics. *Key Eng. Mat*., 2002, **206–213**, 2013.
29. Wagenführ, R., *Holzatlas*. Scientific Publishers, Carl Hanser, Leipzig, 2000.
30. Ness, J. N. and Page, T. F., Microstructural evolution in reaction-bonded silicon carbide. *J. Mat. Sci*., 1986, **21**, 1377.
31. Seo, W.-S. and Koumoto, K., Stacking faults in β-SiC during carbothermal reduction of SiO_2. *J. Am. Ceram. Soc*., 1996, **79**(7), 1777.
32. Schulte-Fischedick, J., Zern, A., Mayer, J., Ruehle, M., Friess, M., Krenkel, W. and ad Kochendorfer, R., The morphology of silicon carbide in C/C-SiC composites. *Mat. Sci. Eng. A*, 2002, **332**, 146.

33. Kim, D. Y., Nishiyama, Y., Wada, M. and Kuga, S., Graphitization of highly crystalline cellulose. *Carbon*, 2001, **39**, 1051.
34. Cheng, H. M., Endo, H., Okabe, K., Saito, K. and Zheng, G. B., Graphitization behaviour of wood ceramics and bamboo ceramics as determined by X-ray diffraction. *J. Porous Mat*., 1999, **6**, 233.
35. Byrne, F. F. and Marsh, H., Introductory overview. In *Porosity in Carbons*, ed. J. W. Patrick. Edward Arnold, London, 1995.
36. Xu, Y., Cheng, L. and Zhang, L., Carbon/silicon carbide composites prepared by chemical vapor infiltration combined with silicon melt infiltration. *Carbon*, 1999, **37**, 1179.
37. Pampuch, R., Walasek, E. and Białosórski, J., Reaction mechanism in carbon-liquid silicon systems at elevated temperatures. *Ceram. Int*., 1986, **12**, 99.
38. Sawyer, G. R. and Page, T. F., Microstructural characterization of ''REFEL'' (reaction-bonded) silicon carbides. *J. Mat. Sci*., 1978, **13**, 885.
39. Seo, W. S. and Koumoto, K., Morphology and stacking faults in β-Silicon carbide whiskers synthesized by carbothermal reduction. *J. Am. Ceram. Soc*., 2000, **83**, 2584.